MATHEMATICAL MODELING OF LIVER FIBROSIS

AVNER FRIEDMAN

Mathematical Biosciences Institute & Department of Mathematics
The Ohio State University
Columbus, OH 43210, USA

WENRUI HAO

Department of Mathematics
The Penn State University
University Park, PA 16802, USA

ABSTRACT. Fibrosis is the formation of excessive fibrous connective tissue in an organ or tissue, which occurs in reparative process or in response to inflammation. Fibrotic diseases are characterized by abnormal excessive deposition of fibrous proteins, such as collagen, and the disease is most commonly progressive, leading to organ disfunction and failure. Although fibrotic diseases evolve in a similar way in all organs, differences may occur as a result of structure and function of the specific organ. In liver fibrosis, the gold standard for diagnosis and monitoring the progression of the disease is biopsy, which is invasive and cannot be repeated frequently. For this reason there is currently a great interest in identifying non-invasive biomarkers for liver fibrosis. In this paper, we develop for the first time a mathematical model of liver fibrosis by a system of partial differential equations. We use the model to explore the efficacy of potential and currently used drugs aimed at blocking the progression of liver fibrosis. We also use the model to develop a diagnostic tool based on a combination of two biomarkers.

1. **Introduction.** Fibrosis is the formation of excessive fibrous connective tissue in an organ or tissue, which occurs in reparative process or in response to inflammation. The excessive deposition disorganizes the architecture of the organ or tissue, and results in scars that disrupt the function of the organ or tissue. Fibrotic diseases are characterized by abnormal excessive deposition of fibrous proteins, such as collagen, and the disease is most commonly progressive, leading to organ disfunction and failure. Fibrotic diseases may become fatal when they develop in vital organs such as heart, lung, liver and kidney. Systemic sclerosis, an autoimmune disease, is another type of fibrotic disease whereby an area that usually has flexibility and movement thickens and hardens; examples include skin, blood vessels, and muscles which tighten under fibrous deposition. Myocardial infarction, commonly known as the heart attack, occurs when blood flow stops to a part of the heart, causing damage to the heart muscles. In this case a reparative response may initiate cardiac fibrosis. On the other hand, an autoimmune disease, such as Lupus Nephritis, begins with inflammation in the kidney, which may then lead to renal tubulointerstitial fibrosis. In general, no matter what initiates the disease, a reparative process or

response to inflammation, fibrosis in an organ eventually involves both reparative process and response to inflammation.

The reparative process in fibrosis is similar to the process of wound healing. Anti-inflammatory macrophages (M2) secrete TGF-β and PDGF which activate fibroblasts and myofibroblasts to excessively produce collagen. At the same time the M2 macrophages secrete MMP (and its antagonist TIMP) which disrupts the cross-linking in the collagen network and initiates the formation of a scar. On the other hand, in response to inflammation that develops in an organ, monocytes from the blood are induced to immigrate into the organ and differentiate into M1 macrophages. A polarization from M1 to M2 then takes place to promote tissue reparation. The heterogeneity of macrophages and the exchange of M1/M2 polarization have been reported in kidney fibrosis (Ricardo et al. [68], Duffield [18]), in liver fibrosis (Tacke et al. [78], Pellicoro et al. [64]), in cardiac fibrosis (Kong et al. [41]) and in idiopathic pulmonary fibrosis (IPF) (Hao et al. [31] and the references therein).

Proinflammatory macrophages M1 produce IL-12 which activates CD4+ T cells. The activities and heterogeneity of T cells have been reported in kidney fibrosis (Tapmeier et al. [81], Liu et al. [48], Nikolic-Paterson [63]), in liver fibrosis (Connolly et al. [13], Barron et al. [5], Hammerich et al. [27], Liedtke et al. [46]), in cardiac fibrosis (Wei et al. [89]), in pulmonary fibrosis (Shimizu et al. [74], Luzina et al. [54], Kikuchi et al. [39], Wei et al. [89], Lo Re et al. [51]), and in systemic sclerosis (Chizzolini [11]). The opposing effects of Th1/Th2 in fibrotic diseases was considered already in earlier work by Wynn [91].

A key protein in enhancing production of collagen by fibroblasts/myofibroblasts is TGF-β. The activity of TGF-β ligand is mediated by a class of SMAD proteins which form complexes that enter into the nucleus of fibroblast/myofibroblast as transcription factors (Leask et al. [44], Kahn et al. [38], Rosenbloom et al. [69]). TGF-β represents an attractive therapeutic target in the treatment of fibrotic diseases [69].
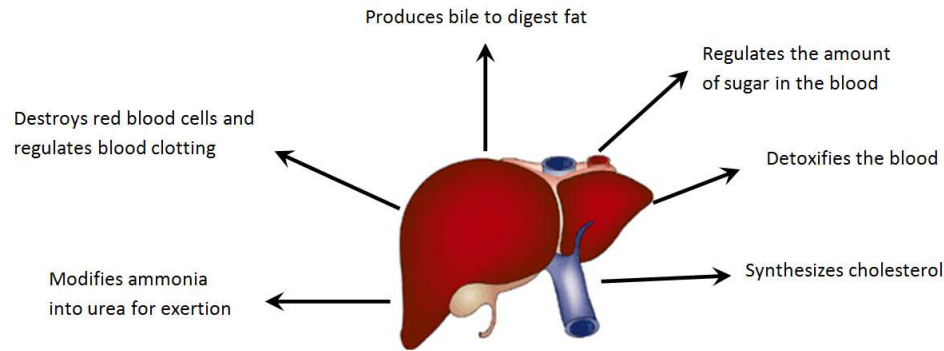

Figure 1. Functions of the liver.

In this paper we focus on liver fibrosis. The liver is an organ that supports the body in many ways, as illustrated in Fig. 1. It produces bile, a substance needed to digest fats which, in particular, helps synthesize cholesterol. It stores sugar glucose and converts it to functional (glucose) sugar when the body sugar levels fall below normal. The liver detoxifies the blood; modifies ammonia into urea for excretion, and destroys old red blood cells. Hepatocytes are the cells of the main parenchymal

tissue of the liver, making up 60% of the total liver cells; they perform most of the tasks of the liver. Kupffer cells are stellar macrophages, in direct contact with the blood, making up 15-20% of the liver cells. Hepatocyte stellate cells (HSCs) are quiescent cells, different from the portal fibroblasts of the liver [17]; they make up 5-8% of the liver cells. The liver walls are lined up with epithelial mesenchymal cells.

Damage to the liver may be caused by toxic drugs, alcohol abuse, hepatitis B and C, or autoimmune diseases. The damage may trigger reparative and inflammatory responses, and the onset of fibrosis. In homeostasis, the HSCs are quiescent cells, but after early liver damage, they become activated [65], producing hyaluronic acid (HA) [3, 4, 24, 73]. HA promotes fibroblast activation and proliferation [23].

The gold standard for diagnosis and monitoring the progression of liver fibrosis is biopsy. But this procedure is invasive and incurs risk, and cannot be repeated frequently. Hence there is currently a great interest in identifying non-invasive markers for diagnosis of liver fibrosis that can detect the pathological progression of the disease [2, 4, 10, 19, 49, 58, 61]. The present paper develops for the first time a mathematical model of liver fibrosis. The model is a continuation and extension of the authors' articles [32, 31] which dealt with kidney fibrosis and lung fibrosis. We use the model to describe the progression of the disease, and identify biomarkers that can be used to monitor treatment for liver fibrosis.

The model is based on the diagram shown in Fig. 1. In Section 2 we list all the variables and proceed to represent the network of Fig. 2 by a system of partial differential equations (PDEs) in a portion of the liver. In Section 3, we simulate the model, and explore potential anti-fibrotic drugs. We also use the mathematical model to quantify the scar density in terms of a combination of two serum biomarkers HA and TIMP, that have been observed in patients [2, 4, 19].

The conclusion of the paper is given in Section 4, and the parameter estimates used in the simulations are given in Section 5. In Section 5 we also perform sensitivity analysis, and in Section 6 we briefly describe the computational method used in the simulations.

2. **Mathematical model.** In this section we develop a mathematical model of liver fibrosis. The fibrosis takes place in some region Ω of the liver. The variables used in the model are given in Table 1. These variables satisfy a system of PDEs in Ω.

Equation for macrophage density. The equation for the density of M1 macrophages is given by

$$\frac{\partial M_1}{\partial t} - D_M \nabla^2 M_1$$
$$= \underbrace{-\nabla \cdot (M_1 \chi_P \nabla P)}_{chemotaxis} + \underbrace{\lambda_{M_1} \frac{\varepsilon_1}{\varepsilon_1 + \varepsilon_2} M_2}_{M_2 \to M_1} - \underbrace{\lambda_{M_2} \frac{\varepsilon_2}{\varepsilon_1 + \varepsilon_2} M_1}_{M_1 \to M_2} \underbrace{-d_{M_1} M_1}_{death},$$

where

$$\varepsilon_1 = \left(\lambda_{MI_\gamma} \frac{I_\gamma}{K_{I_\gamma} + I_\gamma} + \lambda_{MT_\alpha} \frac{T_\alpha}{K_{T_\alpha} + T_\alpha} \right) \frac{1}{1 + I_{10}/K_{I_{10}}},$$
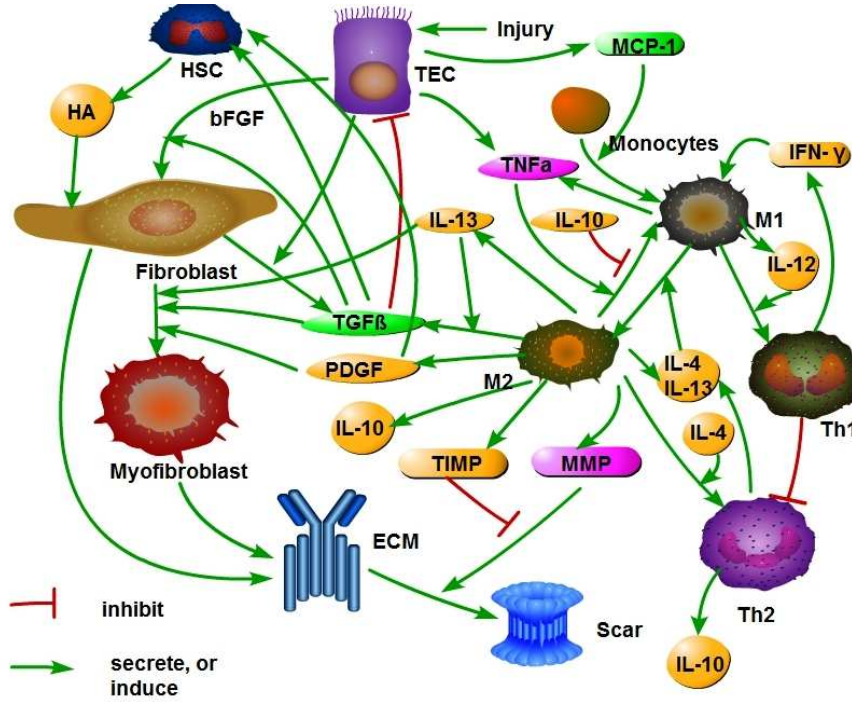$$\varepsilon_2 = \lambda_{MI_4} \frac{I_4}{K_{I_4} + I_4} + \lambda_{MI_{13}} \frac{I_{13}}{K_{I_{13}} + I_{13}}.$$

FIGURE 2. Network of the fibrosis.

TABLE 1. The variables of the model; concentration and densities
are in units of g/cm^3

M_1:	density of M1 macrophages	M_2:	density of M2 macrophages
T_1:	Th1 cell density	T_2:	Th2 cell density
E_0:	density of tissue epithelial cells (TECs)	E	density of activated TECs
H:	density of HSCs	f:	density of fibroblasts
m:	density of myofibroblasts	ρ:	density of ECM
G:	concentration of PDGF	T_β:	concentration of activated TGF-β
Q:	concentration of MMP	Q_r:	concentration of TIMP
T_α	concentration of TNF-α	I_γ	concentration of IFN-γ
I_2:	IL-2 concentration	I_4:	IL-4 concentration
I_{10}:	IL-10 concentration	I_{13}:	IL-13 concentration
P:	concentration of MCP-1	H_A:	Hyaluronic acid concentration
S	scar density		

The term $-\nabla \cdot (M_1 \chi_P \nabla P)$ is the chemotactic effect of MCP-1 on M1 macrophages; χ_P is the chemotactic coefficient.

M2 macrophages may become M1 macrophages under the influence of IFN-γ and TNF-α, a process resisted by IL-10 [15, 33], and M1 macrophage may become M2 macrophages under the influence of IL-4 and IL-13 [84, 85]. Hence the transition between M1 and M2 macrophages depends on the ratio of ε_1 to ε_2: the transition $M_2 \to M_1$ is at rate proportional to $\frac{\varepsilon_1}{\varepsilon_1+\varepsilon_2}$, while the transition $M_1 \to M_2$ is at rate proportional to $\frac{\varepsilon_2}{\varepsilon_1+\varepsilon_2}$. These exchanges of polarization in M1/M2 are expressed by the second and third terms on the right-hand side of the M1 equation.

Macrophages are terminally differentiated cells; they do not proliferate. They differentiate from monocytes that are circulating in the blood and are attracted by MCP-1 into the tissue [86, 88]. Hence they satisfy the boundary condition

$$D_M \frac{\partial M_1}{\partial n} + \tilde{\beta}(P)M_0 = 0 \text{ on the boundary of blood capillaries ,}$$

where $\tilde{\beta}(P)$ depends on MCP-1 concentration, P. Here M_0 denotes the density of monocytes in the blood, i.e., the source of M_1 macrophages from the vascular system. As in [32] we replace the boundary conditions on the blood capillaries by a source term in the tissue, $\beta(P)M_0$.

Then the equation for M1 density in Ω satisfies the equation

$$\frac{\partial M_1}{\partial t} - D_M \nabla^2 M_1 = \beta(P)M_0 - \nabla \cdot (M_1 \chi_P \nabla P) + \lambda_{M_1} \frac{\varepsilon_1}{\varepsilon_1 + \varepsilon_2} M_2$$
$$-\lambda_{M_2} \frac{\varepsilon_2}{\varepsilon_1 + \varepsilon_2} M_1 - d_{M1} M_1. \tag{1}$$

We take $\beta(P) = \beta \frac{P}{K_P + P}$, where β and K_P are constants.

The M2 macrophage density satisfies the equation

$$\frac{\partial M_2}{\partial t} - D_M \nabla^2 M_2 = A_{M_2} + \underbrace{\lambda_{M_2} \frac{\varepsilon_2}{\varepsilon_1 + \varepsilon_2} M_1}_{M_1 \to M_2} - \underbrace{\lambda_{M_1} \frac{\varepsilon_1}{\varepsilon_1 + \varepsilon_2} M_2}_{M_2 \to M_1} \underbrace{-d_{M2} M_2}_{death}, \tag{2}$$

where A_{M_2} accounts for a source of Kupffer cells. The second and third terms on the right-hand side are complimentary to the corresponding terms in Eq. (1).

Equations for T cells density. Naive T cells, T0, are activated as either Th1 by contact with M1 macrophages in an IL-12 environment [37], a process down-regulated by IL-10 [15], or as Th2 cells by contact with M2 macrophages under an IL-4 environment [93]. IL-2 induces proliferation of Th1 cells [29]. Both activation and proliferation of Th1 cells are antagonized by IL-13 [16], while the activation of Th2 cells is antagonized by Th1 [6, 55, 93]. Hence, the equations of Th1 and Th2 densities are given as follows:

$$\frac{\partial T_1}{\partial t} - D_T \Delta T_1 = \left(\lambda_{T_1 M_1} T_0 \frac{M_1}{K_{M_1} + M_1} \frac{I_{12}}{K_{I_{12}} + I_{12}} \frac{1}{1 + I_{10}/K_{I_{10}}} \right.$$
$$\left. + \lambda_{T I_2} \frac{I_2}{K_{I_2} + I_2} T_1 \right) \frac{1}{1 + I_{13}/K_{I_{13}}} \underbrace{-d_{T_1} T_1}_{death}, \tag{3}$$

$$\frac{\partial T_2}{\partial t} - D_T \Delta T_2 = \underbrace{\lambda_{T_2} T_0 \frac{M_2}{K_{M_2} + M_2} \frac{I_4}{K_{I_4} + I_4} \frac{1}{1 + T_1/K_{T_1}}}_{activation}$$
$$\underbrace{-d_{T_2} T_2}_{death}, \tag{4}$$

where T_0 is the density of T0.

Equation for TEC density (E_0 and E). The equation of the inactivated TEC (E_0) density is given by

$$\frac{dE_0}{dt} = A_{E_0} \left(1 + \underbrace{\frac{\lambda_1 E_0 I_D}{K_E + E_0 I_D}}_{repair} \right) - \underbrace{\left(d_{E_0} E_0 + \delta + d_{E_0 T} \frac{T_\beta}{K_{T_\beta} + T_\beta} \right)}_{apoptosis} \underbrace{-\lambda_{E_0} E_0 I_D}_{E_0 \to E}, \tag{5}$$

and the equation for the activated TEC (E) is

$$\frac{dE}{dt} \quad = \quad \underbrace{\lambda_{E_0}E_0 I_D}_{activation} \underbrace{-\lambda_{EM}EI_D}_{EMT} \underbrace{-d_E E}_{death}. \tag{6}$$

In homeostasis, the production of E_0 is represented by the term A_{E_0}, and the death rate is represented by $d_{E0}E_0$. $I_D = 0$, $\delta = 0$ and activated TGF-β concentration is very small. The injury to the epithelium is expressed in two ways: (i) by activation of TEC, which is represented by term $\lambda_{E_0}E_0 I_D$, where D is the damaged region and $I_D = 1$ on D, $I_D = 0$ elsewhere, and (ii) by increased apoptosis caused by oxidative stress [14, 40] (the term with δ) and by TGF-β [63, 70]. The damaged epithelium is partially repaired by fibrocytes, and this is expressed by the term $\frac{\lambda_1 E_0 I_D}{K_D + E_0 I_D}$ [34]. The second term of the right-hand side in Eq. (6) accounts for epithelial mesenchymal transition (EMT) due to injury [63].

Equations for fibroblast concentration (f) and myofibroblast concentration (m). The fibroblasts and myofibroblasts equations are given by:

$$\frac{\partial f}{\partial t} - D_f \nabla^2 f \quad = \quad \underbrace{\lambda_{Ef}E_0}_{source} + \lambda_{fH_A}\frac{H_A}{K_{H_A} + H_A}f$$

$$+ \underbrace{\lambda_{fE}\Big(\frac{T_\beta}{K_{T_\beta} + T_\beta} + \frac{I_{13}}{K_{I_{13}} + I_{13}}\Big)\frac{E}{K_E + E}f}_{production}$$

$$\underbrace{-\Big(\lambda_{mfT}\frac{T_\beta}{K_{T_\beta} + T_\beta} + \lambda_{mfG}\frac{G}{K_G + G}\Big)f}_{f \to m} \underbrace{-d_f f}_{death}, \tag{7}$$

$$\frac{\partial m}{\partial t} - D_m \nabla^2 m \quad = \quad \underbrace{\Big(\lambda_{mfT}\frac{T_\beta}{K_{T_\beta} + T_\beta} + \lambda_{mfG}\frac{G}{K_G + G}\Big)f}_{f \to m} \underbrace{-d_m m}_{death}. \tag{8}$$

The first term on the right-hand side of Eq. (7) is a source from E_0-derived fibroblast growth factor (bFGF), which for simplicity we take to be in the form $\lambda_{Ef}E_0$ [9, 70]. The second term represents the activation and proliferation of fibroblasts by hyaluronic acid [23]. The third term on the right-hand side of Eq. (7) accounts for the fact that TGF-β and IL-13, combined with E-derived bFGF, increase proliferation of fibroblasts [9, 12, 21, 36, 52]. For simplicity, we do not include bFGF specifically in the model, and instead represent it by E. As in [31, 32], TGF-β and PDGF transform fibroblasts into myofibroblasts [20, 52, 59, 66, 77, 82, 92] (the fourth term on the right-hand side of Eq. (7)).

Equation for HSC (H). HSC is activated by PDGF and TGF-β [50]. Hence,

$$\frac{\partial H}{\partial t} - D_H \nabla^2 H \quad = \quad A_H + \underbrace{\Big(\lambda_{HG}\frac{G}{K_G + G} + \lambda_{HT_\beta}\frac{T_\beta}{K_{T_\beta} + T_\beta}\Big)H}_{production} \underbrace{-d_H H}_{death}. \tag{9}$$

Equation for HA (H_A). HA is produced by HSCs and degraded by sinusoidal epithelial cells [3, 4, 19, 24, 73]. Hence,

$$\frac{\partial H_A}{\partial t} - D_{H_A}\nabla^2 H_A \quad = \quad \underbrace{\lambda_{H_A}H}_{production} \quad \underbrace{-d_{H_A}H_A}_{degradation}. \tag{10}$$

Equation for ECM density (ρ) and scar (S). The ECM consists primarily of fibrillar collagen and elastin, but includes also fibronectin, lamina and nitrogen that support the matrix network by connecting or linking collagen (Lu et al. [53]). For simplicity, we represent the ECM by the density of collagen. ECM is produced by fibroblasts, myofibroblasts [52, 59, 60, 76, 82, 92] and by HSCs whose production rate of ECM is similar to that of myofibroblast[22], and TGF-β enhances the production of ECM by myofibroblasts [43, 47, 52, 59, 82, 92]. MMP (Q), in fibrosis, degrades collagen by cutting the protein into small fragments (Veidal et al. [83]); we assume that the loss of collagen is proportional to $Q\rho$. The equation for the density of ECM is then given by:

$$\frac{\partial \rho}{\partial t} \quad = \quad \underbrace{\lambda_{\rho f} f\left(1 - \frac{\rho}{\rho_0}\right)^+ + \lambda_{\rho m}\left(1 + \lambda_{\rho T_\beta}\frac{T_\beta}{K_{T_\beta} + T_\beta}\right)(m + H)}_{production}$$
$$-d_{\rho Q}Q\rho \underbrace{-d_\rho \rho}_{death}, \tag{11}$$

where $\left(1 - \frac{\rho}{\rho_0}\right)^+ = 1 - \frac{\rho}{\rho_0}$ if $\rho < \rho_0$, $\left(1 - \frac{\rho}{\rho_0}\right)^+ = 0$ if $\rho \geq \rho_0$. There are several computational models of collagen network under various biological conditions (Lee et al. [45]) and under strain-dependent degradation (Hadi et al. [25]). But the parameters used in these models are not helpful in determining how scar develops by excess of ECM while under the effect of MMP. Since MMP increases scarring in cases of excessive collagen concentration, we shall use the following simple formula to describe the the growth of a scar:

$$S = \lambda_S(\rho - \rho^*)^+\left(1 + \lambda_{SQ}\frac{Q}{K_Q + Q}\right), \tag{12}$$

where ρ^* is the concentration of collagen in normal healthy tissue and λ_S, λ_{SQ} and K_Q are positive parameters.

Equation for MCP-1 (P). The MCP-1 equation is given by

$$\frac{\partial P}{\partial t} - D_P\nabla^2 P \quad = \quad \underbrace{\lambda_{PE}E}_{production} \underbrace{-d_{PM}\frac{P}{K_P + P}M_1 - d_P P}_{degradation}, \tag{13}$$

where λ_{PE} represents the growth rate by activated TEC following damage to the endothelium [32, 34, 35, 71, 72, 75, 88, 87]. The second term on the right-hand side accounts for the internalization of MCP-1 by macrophage, which is limited due to the limited rate of receptor recycling.

Equations for concentrations of PDGF (G), MMP (Q), and TIMP (Q_r). These cytokines are produced by macrophages [86, 94] and, as in [32], the following sets

of diffusion equations hold for G, Q and Q_r:

$$\frac{\partial G}{\partial t} - D_G \nabla^2 G \quad = \quad \underbrace{\lambda_{GM} M_2}_{production} \quad \underbrace{-d_G G}_{degradation} \quad , \tag{14}$$

$$\frac{\partial Q}{\partial t} - D_Q \nabla^2 Q \quad = \quad \underbrace{\lambda_{QM} M_2}_{production} \underbrace{-d_{QQ_r} Q_r Q}_{depletion} \underbrace{-d_Q Q}_{degradation} \quad , \tag{15}$$

$$\frac{\partial Q_r}{\partial t} - D_{Q_r} \nabla^2 Q_r \quad = \quad \underbrace{\lambda_{Q_r M} M_2}_{production} \underbrace{-d_{Q_r Q} Q Q_r}_{depletion} \underbrace{-d_{Q_r} Q_r}_{degradation} \quad . \tag{16}$$

Note that in Eq. (15), MMP is lost by binding with TIMP (second term), a process which also depletes TIMP in Eq. (16).

Equations for concentrations of TGF-β (T_β) and TNF-α (T_α). TGF-β is produced and is activated by M2 macrophages, a process jointly enhanced by IL-13 [12, 21, 36, 80]; in addition, TGF-β is produced and is activated by TECs and fibroblasts [8, 70]. Hence T_β satisfies the equation:

$$\frac{\partial T_\beta}{\partial t} - D_{T_\beta} \nabla^2 T_\beta = \underbrace{\lambda_{T_\beta M} M_2 \Big(1 + \lambda_{T_\beta I_{13}} \frac{I_{13}}{I_{13} + K_{I_{13}}}\Big) + \lambda_{T_\beta f} f \frac{E}{E + K_E}}_{production} \underbrace{-d_{T_\beta} T_\beta}_{degradation} \quad . \tag{17}$$

TNF-α is produced by M1 macrophages [67], and by TEC [8, 57], and is depleted when it combines with receptors on M2 in the process which produces phenotype exchange $M_2 \to M_1$:

$$\frac{\partial T_\alpha}{\partial t} - D_{T_\alpha} \nabla^2 T_\alpha \quad = \quad \underbrace{\lambda_{T_\alpha M} M_1 + \lambda_{T_\alpha E} E}_{production} \underbrace{-\lambda_{MT_\alpha} \frac{T_\alpha}{K_{T_\alpha} + T_\alpha} M_2}_{M_2 \to M_1} \underbrace{-d_{T_\alpha} T_\alpha}_{degradation} \quad . \tag{18}$$

Equation for interleukins: IL-2 is produced by Th1 cells [29]:

$$\frac{\partial I_2}{\partial t} - D_{I_2} \Delta I_2 \quad = \quad \underbrace{\lambda_{I_2 T_1} T_1}_{production} \underbrace{-d_{I_2} I_2}_{degradation} \quad . \tag{19}$$

IL-4 is produced by Th2 cells and M2 macrophages [6, 55], hence

$$\frac{\partial I_4}{\partial t} - D_{I_4} \Delta I_4 \quad = \quad \underbrace{\lambda_{I_4 T_2} T_2 + \lambda_{I_4 M_2} M_2}_{production} \underbrace{-d_{I_4} I_4}_{degradation} \quad . \tag{20}$$

IL-10 is produced primarily by M2 macrophages, while IL-12 is produced primarily by M1 macrophages in a process that is s antagonized by IL-10 [15] and IL-13 [1]. Hence IL-10 and IL-12 satisfy the equations:

$$\frac{\partial I_{10}}{\partial t} - D_{I_{10}} \Delta I_{10} \quad = \quad \underbrace{\lambda_{I_{10} M_2} M_2}_{production} \underbrace{-d_{I_{10}} I_{10}}_{degradation} , \tag{21}$$

$$\frac{\partial I_{12}}{\partial t} - D_{I_{12}} \Delta I_{12} \quad = \quad \underbrace{\lambda_{I_{12} M_1} M_1 \frac{1}{1 + I_{10}/K_{I_{10}}} \frac{1}{1 + I_{13}/K_{I_{13}}}}_{production} \underbrace{-d_{I_{12}} I_{12}}_{degradation} \quad . \tag{22}$$

IL-13 is produced by M2 macrophages [28, 68] and by Th2 cells [79, 84], so that

$$\frac{\partial I_{13}}{\partial t} - D_{I_{13}}\Delta I_{13} \;=\; \underbrace{\lambda_{I_{13}T_2}T_2 + \lambda_{I_{13}M}M_2}_{production} \underbrace{-d_{I_{13}}I_{13}}_{degradation}. \tag{23}$$

2.1. Equations for IFN-γ (I_γ): IFN-γ is produced by Th1 cells [29]:

$$\frac{\partial I_\gamma}{\partial t} - D_{I_\gamma}\Delta I_\gamma \;=\; \underbrace{\lambda_{I_\gamma T_1}T_1}_{production} -d_{I_\gamma}I_\gamma. \tag{24}$$

The parameters which appear in Eqs (1)-(21) are listed in Tables 2-4 of Section 5 together with their dimensional values.

3. **Results.** A model of of renal fibrosis was introduced by Hao et al. [32]. The model combines M1 and M2 macrophages into one variable M, and does not include T cells. Based on patients' data, the model suggests that urine measurements of (TGF-β, MCP-1) could serve as biomarkers to determine the severity of the disease. The lung contains many tiny alveoli, where oxygen is absorbed. The tissue surrounding them is the lung interstitium. Idiopathic pulmonary fibrosis (IPF) is a fibrosis of the interstitium whose etiology is unknown. A model of IPF was developed by Hao et al. [31] takes into account of the unique alveoli structure of the lung. The model includes the alveolar macrophages (M2) and the proinflammatory macrophages (M1) but, it does include T cells.

The model developed in the present paper is more comprehensive than the models developed in [31, 32] since it includes T cells, and liver-specific cells, namely HSCs, as well as the hyaluronic acid (HA), produced by HSCs; both HSCs and HA play important roles in liver fibrosis. By including T cells and HSCs we can explore potential anti-fibrotic drugs such as injection of IFN-γ, and potential serum biomarkers such as HA.

Boundary conditions. We assume that fibrosis occurs only within the region Ω, hence:

$$\text{all the variables satisfy non-flux condition on the boundary of } \Omega. \tag{25}$$

Initial conditions. We take the following initial conditions (mostly from [32, 33]):

$$M_1 = 3.73 \times 10^{-5} \; g/ml, \; M_2 = 3.38 \times 10^{-5} \; g/ml, \; T_1 = 4.83 \times 10^{-5} \; g/ml,$$
$$T_2 = 2.37 \times 10^{-5} \; g/ml, \; E_0 = 0.1 \; g/ml, \; E = 1 \times 10^{-6} \; g/ml,$$
$$f = 1.2 \times 10^{-2} \; g/ml, \; m = 7.1 \times 10^{-6} \; g/ml, \; \rho = 0.002 \; g/ml$$
$$P = 5.59 \times 10^{-8} \; g/ml, \; G = 3.07 \times 10^{-10} \; g/ml, \; Q = 2.29 \times 10^{-6} \; g/ml,$$
$$Q_r = 10^{-6} \; g/ml, \; T_\beta = 1.52 \times 10^{-9} \; g/ml, \; T_\alpha = 1.47 \times 10^{-9} \; g/ml,$$
$$I_2 = 2.49 \times 10^{-8} \; g/ml, \; I_4 = 3.22 \times 10^{-12} \; g/ml, \; I_{13} = 1.13 \times 10^{-9} \; g/ml,$$
$$I_{10} = 7.66 \times 10^{-12} \; g/ml, \; I_{12} = 1.64 \times 10^{-8} \; g/ml, \; \text{and } I_\gamma = 1.82 \times 10^{-11} \; g/ml. \tag{26}$$

We also assume initial homeostasis with a small amount of inflammation represented by the term $\lambda_{PE}E$ in Eq. (13):

$$\lambda_{E_0}E_0 I_D = 0, \; \lambda_{PE}E = \varepsilon_0, \; \varepsilon_0 \text{ is small.} \tag{27}$$

Finally, we take at $t = 0$ homeostasis values of HA (from [7, 19]) and H (from Sec. 5, under Eq. (9)):

$$HA = 10^{-4} \ g/ml, \ H = 0.001 \ g/ml. \tag{28}$$

In the following simulations the parameter values are taken from Tables 2-4. For simplicity, we simulate the model for a 2-d domain Ω, taking

$$\Omega \text{ a square of side 1 cm, and } D \text{ a concentric square of side 0.3 cm.} \tag{29}$$

Fig. 3 shows the dynamics of the average concentrations of cells, cytokines and ECM for the first 200 days. The parameters are taken from Tables 2-4.
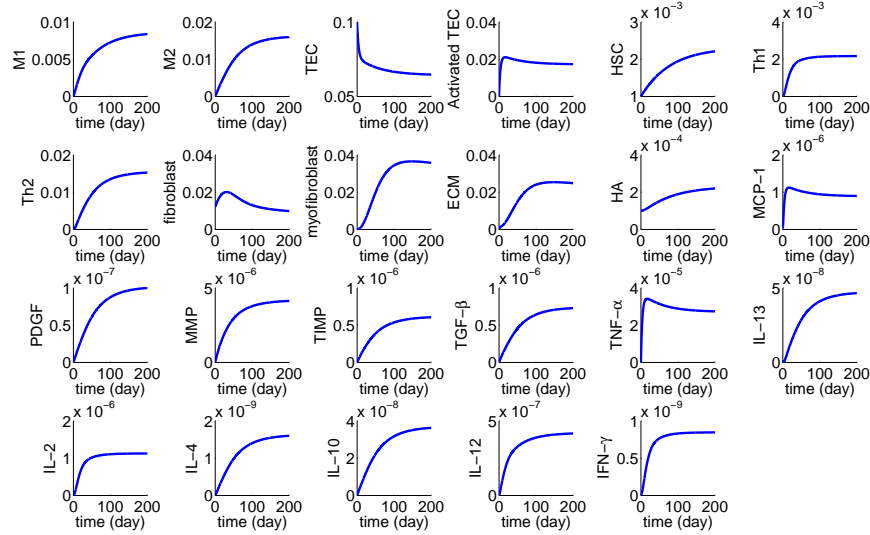

FIGURE 3. The average concentrations of cells, cytokines and ECM

We see that most densities/concenrations nearly stabilize by day 100; however TEC density and fibroblast concentration continue to decrease while the myofibrob-lasts concentration increases. We note that ECM increases up to 6 times its initial value for healthy case, in agreement with [19].

We are mostly interested in scar formation, hence in scar density S. The parameters in Eq. (12) are unknown, and for illustration we take $\lambda_S = 100$, $\lambda_{SQ} = 1$ and $K_Q = 5 \times 10^{-6}$ in Eq. (12). The profile of the scar density $S(t)$ for the first 200 days is shown by the blue curve in Fig. 4. We see that $S(t)$ grows initially fast, but the growth rate gradually decreases. Other choices of the parameters λ_S, λ_{SQ} and K_Q show the same qualitative behavior.

Treatment studies. We can use the model to explore potential drugs. We express the effect of a drug indirectly by either reducing some of the parameters in the relevant equations by factors such as $\frac{1}{1+A}$, $\frac{1}{1+B}$, θ, or by adding a constant term c in the relevant equation during the treatment period. The choices of A, B and c are somewhat arbitrary, since they depend on the actual amount of dozing. Such drugs could be, for instance, anti-TGF-β, NOX inhibitor or IFN-γ injection. Fig. 4 displays the effect of treatment when the drug is administered at day 100 for 100
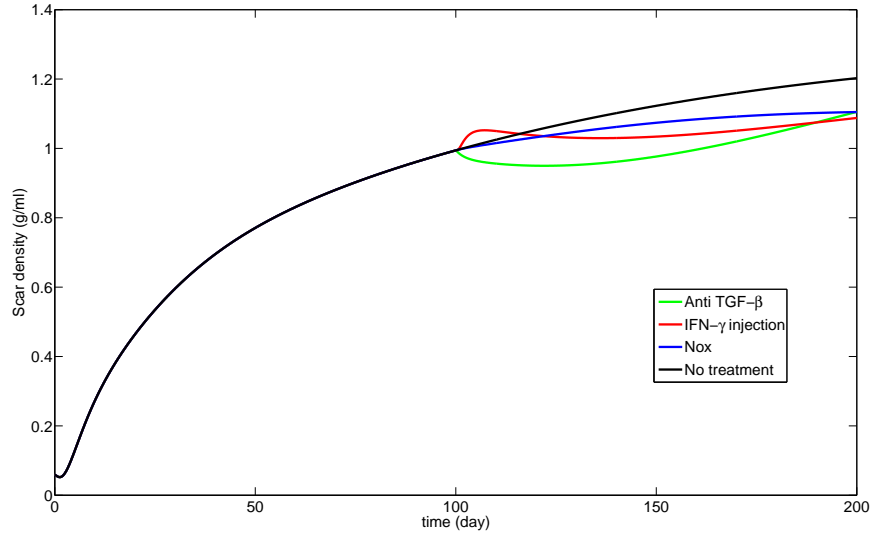
FIGURE 4. Treatment studies

days, continuously. We determine the efficacy of the drug by how much it blocks or reduces the scar density.

Anti-TGF-β. We first consider an anti-TGFβ drug, such as Pirfenidone which was recently approved in the United States. In our model we need to replace $\lambda_{T_\beta M}$ and $\lambda_{T_\beta f}$ by $\lambda_{T_\beta M}/(1 + A)$ in Eq. (17) and $\lambda_{T_\beta f}/(1 + A)$, and T_β by $T_\beta/(1 + B)$ in all terms where T_β acts to promote fibrosis. The green curve in Fig. 4 shows the effect of the drug for $A = B = 0.1$. We see that in terms of scar, the drug is initially effective in decreasing the scar density, but in the long term its effect diminishes.

NOX inhibitor. One of suggested novel drugs for treatment of hepatic fibrosis is NOX inhibitor [42]. NOX are membrane proteins that activate HSCs [65]. The effect of anti NOX drug is to decrease λ_{HG} and λ_{HT_β} in Eq. (9) by a factor of $\theta \in (0, 1]$; $\theta = 1$ when no drug is applied. The black curve in Fig. 4 shows the dynamics of the scar for $\theta = 0.5$ and suggests that the drug may be very effective as anti-fibrotic drug. Micro RNA-21 (miR-21) modulates ERK1 signaling in HSCs activation and is overexpressed in hepatic fibrosis [95]. Anti miR-21 is a potential anti-fibrotic drug which, in our model, has the same effect as NOX inhibitor.

Injection of IFN-γ. It was suggested by Weng et al. [90] that IFN-γ treatment may reduce liver fibrosis. Such a treatment means that we need to add in our model a source term c in Eq. (24) to represent the injection of IFN-γ. Taking $c = 10^{-9}$ g/ml/day, we see, in Fig. 4, that the drug initially promotes fibrosis but later on it reverses fibrosis. This behavior may be attributed to the fact that fibrosis has both non-inflammatory reparative aspect and proinflammatory aspect. Hence IFN-γ injection can affect the disease in either negative and positive ways.

Biomarkers. Patients with liver fibrosis have higher concentration of HA and TIMP in the liver [2, 4, 19]. We can use the mathematical model to develop a diagnostic tool to determine the state of the disease based on combined measurements of HA and TIMP. We do not know when the disease of an individual patient
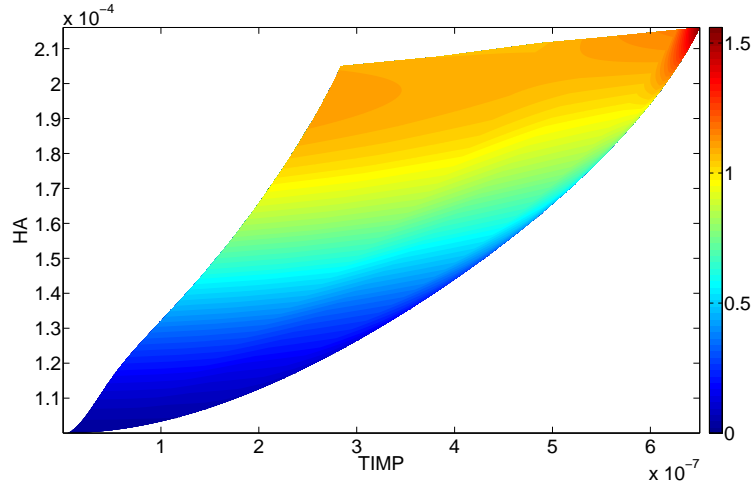
FIGURE 5. Biomarkers HA and TIMP with respect to scar density;
the color column scales the scar density in g/cm^3.

began, or equivalently, what was the damaged area D of an individual patient at
time $t = 0$ when the biomarkers were measured. Hence we take D to be a rectangle
with variable side λ, where $\lambda \in [0.2, 0.9]$ depends on the individual patient.

For each λ we simulate the model for time $0 \leq t \leq 200$ days and determine the
quantities $HA(t, \lambda)$, $TIMP(t, \lambda)$ and the scar density $S(t, \lambda)$. As λ increases, the
curves $\Gamma(\lambda) = \{HA(t, \lambda), TIMP(t, \lambda), \quad 0 \leq t \leq 200\}$ increase and span a region in
the $HA - TIMP$ plane shown in Fig. 5. We associate to each point in this region
the corresponding value of $S(t, \lambda)$, using color from the color column in Fig. 5. Fig.
5 can then be used to determine, for any individual, based on his/her concentrations
of HA and TIMP in the liver, what the scar density is.

As reported in [26, 61, 62], the serum biomarkers of HA and TIMP reflect the
disease state, and thus roughly the tissue levels of HA and TIMP. As the corre-
lation between tissue and serum concentrations of HA and of TIMP become more
precise, Fig. 5 could then provide a quantitative non-invasive diagnostic tool for
liver fibrosis.

We note however that some of the parameters in the model equations may not be
sufficiently precise; there are also variations from one person to another. Sensitivity
analysis (such as that carried in Sec 5.1) shows that the scar density varies in a
continuous way when parameters are changed continuously within a limited range.
Hence Fig. 5 should be viewed as just one possible prediction map; similar maps
could be produced with other parameters. When new experimental and clinical
data become available, some of the parameters, especially these under "estimated"
in Tables 2-4, could be modified to make simulations better fit the data. Sensitivity
analysis could be used in order to modify collectively a group of parameters.

4. **Conclusion.** Fibrosis in an organ is characterized by excessive deposition of
fibrous connective tissue. It disorganizes the architecture of the organ, leading to
the formation of scars and eventual disfunction and failure of the organ. There
are currently no drugs that can appreciably reverse the progress of the disease.

The present paper focuses on liver fibrosis. The gold standard for diagnosis and monitoring the pathological progression of liver fibrosis is biopsy. But this procedure is invasive and incurs risk, and cannot repeated frequently. For this reason we developed, for the first time, a mathematical model that describes the progression of the disease and the effect of drug treatment, and we used the model to construct a diagnostic map based on a combination of biomarkers. The model is represented by a system of 24 partial differential equations for the concentrations of cells and cytokines. The cells are macrophages M1 and M2, T cells Th1 and Th2, fibroblasts, myofibroblasts, HSCs, and tissue epithelial cells. The cytokines are either produced by these cells, or affect the activities of the cells. The mathematical model builds on the models developed in [31, 32], but it also includes HSCs and CD4+ T cells: Th1 and Th2. This extended model enables us to explore new potential drugs. For example, we tested with our model the efficacy of treatment by injection of IFN-γ, a suggestion made in [90]. We found, interestingly, that the drug initially increases fibrosis but later on decreases it.

We used the model to explore the efficacy of other potential drugs aimed to block liver fibrosis. Currently, most of the available data on anti-fibrotic drugs are obtained from mice experiments. As more clinical data become available, our model could be refined (by modifying some of the parameters) and validated, and it could then serve as as useful tool in exploring the efficacy of anti-fibrotic drugs for the treatment of liver fibrosis in human patients.

There is currently a great interest in determing reliable serum biomarkers for diagnosis and prognosis of liver fibrosis [2, 4, 10, 19, 49, 58, 61]. Our mathematical model can be used as diagnostic and prognostic tool by using a combination of two biomarkers. Thus, in Fig. 5 we quantified the dependence of scar density in liver fibrosis in terms of concentrations of TIMP and HA in the fibrotic tissue; these two concentrations are overexpressed in serum of patients with liver fibrosis [19, 61]. Our model can be used to explore other combinations of biomarkers in liver fibrosis as more experimental and clinical data become available.

5. **Parameters.** The parameters of the model are listed in Tables 2-4. Most of the parameter are taken from previous works [29, 30, 30, 32, 33]. The remaining parameters are estimated below.

Eq. (3). In the blood of a healthy adult there are 5000,000-750,000 T cells per ml, which translates into an average of approximately 5×10^{-4}g/ml. We assume that the density of naive CD4+ T cells in the tissue is significantly smaller, taking $T_0 = 3 \times 10^{-5}$ g/ml.

Eq. (4). The production of T_1 by M_1 under I_{12} environment is $\lambda_{T_1 M_1} = 10$/day [33]. We assume that the production of T_2 by M_2 under I_4 environment is much smaller, taking $\lambda_{T_2} = 0.75$/day.

Eq. (5). We assume that the density of E_0 of the inactivated epithelial cells in the liver is 0.1 g/ml. The repair term A_{E_0} was estimated in [32] to be 8.27×10^{-3} g/ml/day. We assume that the repair is 5 times slower in the liver, taking $A_{E_0} = 1.65 \times 10^{-3}$ g/ml/day.

Eq. (7). The production rate of fibroblasts by activated TEC is 5×10^{-4}/day [32]. We assume that the production of fibroblasts by HSC-produced HA is five times larger, taking, $\lambda_{fH_A} = 2.5 \times 10^{-3}$/day. The transition rate from fibroblasts to myofibroblasts, λ_{mfT} and λ_{mfG}, in the lung were estimated in [32] by 0.12/day.

We assume these rates are larger in the liver than in the lung, taking $\lambda_{mfT} = \lambda_{mfG} = 0.3$/day.

Eq. (9). HSCs make up 5-8% of all the liver tissue. Accordingly we take $H = 0.02$ g/ml. We assume that in homeostasis only 5% HSCs are activated, that is, $H = 0.001$ g/ml. The death rate of HSCs is assumed to be the same as for fibroblast, $d_H = d_f = 1.66 \times 10^{-2}$ day^{-1}. From the steady state equation $A_H - d_H H = 0$, we then get, $A_H = 1.66 \times 10^{-5}$ g/ml/day.

We take $\lambda_{HG} = \lambda_{HT_\beta}$ and assume that, when activated, the number of HSC increased by 25%. We account for this by taking $\lambda_{GH} = \lambda_{T_\beta H} = 0.2 d_H = 3.32 \times 10^{-3}$ day^{-1}.

Eq. (10). We assume the degradation rate of HA by sinusoidal epithelial cells to be $d_{H_A} = 0.29$/day [7]. In health the concentration of HA is 10^{-4} g/ml [7, 19]. From the steady state equation

$$\lambda_{H_A} H - d_{H_A} H_A = 0,$$

with $H = 0.001$, we then get $\lambda_{H_A} = 2.9 \times 10^{-2}$ day^{-1}.

Eq. (15). The production of MMP and TIMP by M2 macrophage in the lung was taken in [33] to be 3×10^{-4}/day and 6×10^{-5}/day, respectively. We assume that the production rate is larger in the liver, taking $\lambda_{QM} = 3 \times 10^{-3}$/day and $\lambda_{Q_r M} = 6 \times 10^{-4}$/day.

5.1. **Sensitivity analysis.** We performed sensitivity analysis on some of the production parameters of the system (1)-(17). Following the method in [56], we performed Latin hypercube sampling and generated 1000 samples to calculate the partial rank correlation (PRCC) and the p-values with respect to the scar concentration at day 200. The results are shown in Fig. 6 (The p-value was < 0.01).

Scar density grows if ρ and Q are increased (Eq. (12) and ρ increases with increase in f, m, H and T_β (Eqs. (11), (12)); f is increased by H_A which is produced by H. These observations explain why the parameters λ_{HG}, λ_{HT_β}, λ_{H_A}, $\lambda_{T_\beta M}$ and $\lambda_{T_\beta I_{13}}$ are positively correlated. We next observe that T_β is produced by M_2 (and f), hence the transition $M_1 \rightarrow M_2$ positively affects scar growth. This transition is increased if T_α is decreased while I_{10} and I_{13} are increased (see the form of ε_1, ε_2 which appear in Eqs. (1), (2)). Hence $\lambda_{I_{10}M_2}$, $\lambda_{I_{13}T_2}$ and λ_{MT_α} are positively correlated while $\lambda_{T_\alpha M}$ is negatively correlated (see Eq. (18)). Since MCP-1 attracts macrophages to the liver, the production rate of MCP-1 by TEC, λ_{PE}, is positively correlated. The sensitivity analysis can be carried out in a similar way for the remaining production parameters.

6. **Computational method.** In order to illustrate our numerical method, we consider the following diffusion equation:

$$\frac{\partial X}{\partial t} - D_X \nabla^2 X = F_X \text{ in } \Omega, \tag{30}$$

where the right-hand side accounts for all the 'active' terms. Let $X_{i,j}^n$ denote a numerical approximation of $X(ih_x, jh_y, n\tau)$, where h_x and h_y are the stepsize in
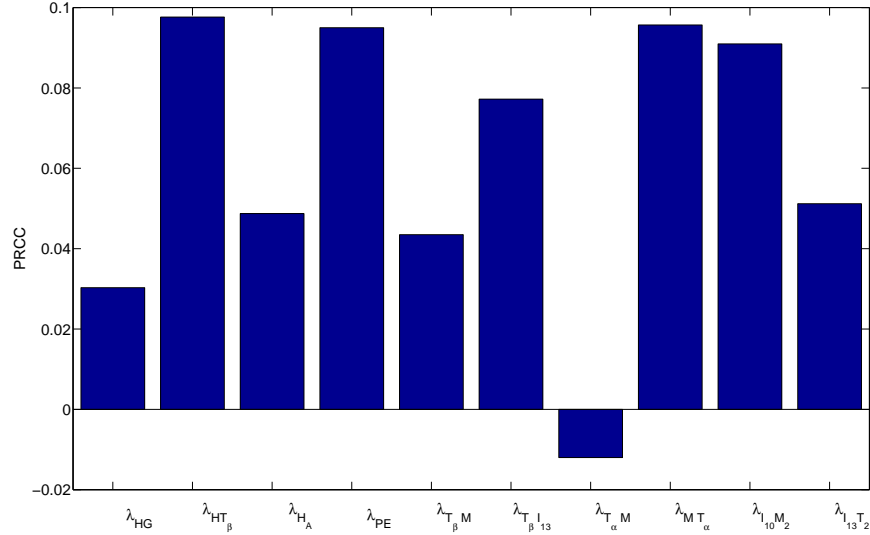
FIGURE 6. The sensitivity analysis for the cytokine production rates. The figure shows the partial rank correlation (PRCC) between the cytokine production rate and the scar concentration at day 200.

the x and y directions respectively, and τ is the time stepsize. Then a discretization is derived by the explicit Euler five-point finite difference scheme, i.e.,

$$\frac{X_{ij}^{n+1} - X_{ij}^n}{\tau} - D_X \left(\frac{X_{i+1,j}^n + X_{i-1,j}^n - 2X_{i,j}^n}{h_x^2} + \frac{X_{i,j+1}^n + X_{i,j-1}^n - 2X_{i,j}^n}{h_y^2} \right)$$
$$= F_X(X_{i,j}^n) \text{ in } \Omega. \tag{31}$$

In order to make the scheme stable, we take $\tau \leq \frac{h^2}{4D_X}$, namely $\tau = 0.1\frac{h^2}{D_X}$, where $h = h_x = h_y$.

REFERENCES

[1] B. C. A. and R. J.-P., *Cytokines and Cytokine Receptors: Physiology and Pathological Disorders*, CRC Press.

[2] L. A. Adams, Biomarkers of liver fibrosis, *J. Gastroenterol Hepatol*, **26** (2011), 802–809.

[3] S. Albeiroti, K. Ayasoufi, D. R. Hill, B. Shen and C. A. de la Motte, Platelet hyaluronidase-2: An enzyme that translocates to the surface upon activation to function in extracellular matrix degradation, *Blood*, **125** (2015), 1460–1469.

[4] A. Baranova, P. Lal, A. Birerdinc and Z. M. Younossi, Non-invasive markers for hepatic fibrosis, *BMC Gastroenterol*, **11** (2011), 91.

[5] L. Barron and T. A. Wynn, Fibrosis is regulated by Th2 and Th17 responses and by dynamic interactions between fibroblasts and macrophages, *Am. J. Physiol. Gastrointest. Liver Physiol.*, **300** (2011), G723–728.

[6] D. C. Baumgart and S. R. Carding, Inflammatory bowel disease: Cause and immunobiology, *Lancet*, **369** (2007), 1627–1640.

TABLE 2. Parameters' description and value

Parameter	Description	Value
D_M	dispersion coefficient of macrophages	8.64×10^{-7} cm^2 day^{-1}[32]
D_T	diffusion coefficient of T cell	8.64×10^{-7} cm^2 day^{-1}[33]
D_{I_γ}	diffusion coefficient of IFN-γ	1.08×10^{-2} cm^2 day^{-1}[29]
D_{I_2}	diffusion coefficient of IL-2	1.08×10^{-2} cm^2 day^{-1}[29]
D_{I_4}	diffusion coefficient of IL-4	1.08×10^{-2} cm^2 day^{-1}[29]
$D_{I_{12}}$	diffusion coefficient of IL-12	1.08×10^{-2} cm^2 day^{-1}[29]
$D_{I_{13}}$	diffusion coefficient of IL-13	1.08×10^{-2} cm^2 day^{-1}[29]
D_P	diffusion coefficient of MCP-1	1.728×10^{-1} cm^2 day^{-1}[32]
D_G	diffusion coefficient of PDGF	8.64×10^{-2} cm^2 day^{-1}[32]
D_Q	diffusion coefficient of MMP	4.32×10^{-2} cm^2 day^{-1}[32]
D_{Q_r}	diffusion coefficient for TIMP	4.32×10^{-2} cm^2 day^{-1} [32]
D_{T_β}	diffusion coefficient for TGF-β	4.32×10^{-2} cm^2 day^{-1} [32]
D_{T_α}	diffusion coefficient for TNF-α	1.29×10^{-2} cm^2 day^{-1}[31]
D_f	dispersion coefficient of fibroblasts	1.47×10^{-6} cm^2 day^{-1} [32]
D_m	dispersion coefficient of myofibroblasts	1.47×10^{-5} cm^2 day^{-1} [32]
λ_{M2}	Differentiation rate of M1 to M2	0.3 day^{-1} [33]
λ_{M1}	Maximal rate at which M2 is activated to become M1	0.6/day [33]
λ_{MT}	transition rate of M2 to M1 macrophages by TNF-α	5×10^{-3} day^{-1} [15]
λ_{MI_r}	Production rate by IFN-γ	1/day [33]
λ_{MI_4}	Production rate by IL-4	1/day [33]
$\lambda_{MI_{13}}$	Production rate by IL-13	1/day [33]
λ_{T1M1}	Production rate of Th1 cells by M1 macrophages	10/day [33]
λ_{T1I2}	Production rate of Th1 cells by IL-12	1/day [29]
λ_{T2}	Production rate of Th2 cells by M1	0.75/day estimated
λ_{E_0}	production rate of AEC	0.25 day^{-1} [31]
λ_1	repair rate of AEC	10^{-3} g/cm^3 day^{-1} [31]
λ_{EM}	EMT rate of AEC	1.65×10^{-3} day^{-1} [31]
λ_{HG}	production rate of HSCs by PDGF	1.5×10^{-3} day^{-1} estimated
λ_{HT_β}	production rate of HSCs by TGF-β	3.32×10^{-3} day^{-1} estimated
$\lambda_{H_A H}$	production rate of HA by HSCs	2.9×10^{-2} day^{-1} estimated
$\lambda_{T_\beta M}$	production rate of TGF-β by macrophages	1.5×10^{-2} day^{-1} [32]
$\lambda_{T_\beta f}$	production rate of TGF-β by fibroblast	7.5×10^{-3} day^{-1} [31]
$\lambda_{T_\beta I_{13}}$	production rate of TGF-β by IL-13	2 [31]
λ_{GM}	production rate of PDGF by macrophages	2.4×10^{-5} day^{-1} [32]
λ_{QM}	production rate of MMP by macrophages	2×10^{-3} day^{-1} estimated
$\lambda_{Q_r M}$	production rate of TIMP by macrophages	4×10^{-4} day^{-1} estimated
λ_{PE}	activation rate of MCP-1 due to AECs	1×10^{-8} day^{-1} [32]
$\lambda_{\rho f}$	activation rate of ECM due to fibroblasts	3×10^{-3} day^{-1} [32]
$\lambda_{\rho m}$	activation rate of ECM due to myofibroblasts	6×10^{-3} day^{-1} [32]
$\lambda_{\rho T_\beta}$	activation rate of ECM due to TGF-β	2 [32]
λ_{Ef}	activation rate of fibroblasts due to bFGF and TGF-β	2.5×10^{-1} day^{-1} [31]
$\lambda_{f H_A}$	production rate of fibroblasts by HA	2.5×10^{-3} day^{-1} estimated
λ_{fE}	production rate of fibroblasts	5×10^{-4} day^{-1} [31]
λ_{mfT}	activation rate of myofibroblasts due to TGF-β	0.3 day^{-1} estimated
λ_{mfG}	activation rate of myofibroblasts due to PDGF	0.3 day^{-1} estimated

[7] K. D. Bentsen, J. H. Henriksen, S. Boesby, K. Horslev-Petersen and I. Lorenzen, Hepatic and renal extraction of circulating type III procollagen amino-terminal propeptide and hyaluronan in pig, *J. Hepatol.*, **9** (1989), 177–183.

[8] C. E. Boorsma, C. Draijer and B. N. Melgert, Macrophage heterogeneity in respiratory diseases, *Mediators Inflamm.*, **2013** (2013), 769214, 19pp.

[9] A. Camelo, R. Dunmore, M. A. Sleeman and D. L. Clarke, The epithelium in idiopathic pulmonary fibrosis: breaking the barrier, *Front Pharmacol*, **4** (2014), 173.

[10] A. Cequera and M. C. Garcia de Leon Mendez, [Biomarkers for liver fibrosis: Advances, advantages and disadvantages], *Rev Gastroenterol Mex*, **79** (2014), 187–199.

[11] C. Chizzolini, T cells, B cells, and polarized immune response in the pathogenesis of fibrosis and systemic sclerosis, *Curr Opin Rheumatol*, **20** (2008), 707–712.

TABLE 3. Parameters' description and value

Parameter	Description	Value
$\lambda_{T_\alpha M}$	activation rate of TNF-α due to macrophage	1.39×10^{-2} day^{-1} [31]
$\lambda_{T_\alpha E}$	activation rate of TNF-α due to macrophage	6.9×10^{-4} day^{-1} [31]
$\lambda_{I_2 T_1}$	production rate of IL-2 by Th1 cells	4.2×10^{-4} day^{-1} [33]
$\lambda_{I_4 T_2}$	production rate of IL-10 by Th2 cells	5.96×10^{-4} day^{-1} [33]
$\lambda_{I_4 M_2}$	production rate of IL-10 by M2 macrophages	2.38×10^{-3} day^{-1} [33]
$\lambda_{I_{10} M2}$	production rate of IL-10 by M2 macrophages	6.67×10^{-4} day^{-1} [33]
$\lambda_{I_{12} M_1}$	production rate of IL-12 by M1 macrophages	9.64×10^{-2} day^{-1} [33]
$\lambda_{I_{13} T_2}$	production rate of IL-13 by Th2 cells	2.24×10^{-4} day^{-1} [33]
$\lambda_{I_{13} M_2}$	production rate of IL-13 by macrophages	5.94×10^{-4} day^{-1} [33]
$\lambda_{I_r T_1}$	production rate of IFN-γ by Th1 cells	2.87×10^{-5} day^{-1} [33]
d_{M_2}	death rate of macrophages	0.015 day^{-1} [32]
d_{M_1}	death rate of macrophages	0.02 day^{-1} [31]
d_{T_1}	death rate of Th1 cell	1.97×10^{-1} day^{-1} [33]
d_{T_2}	death rate of Th2 cell	1.97×10^{-1} day^{-1} [33]
d_E	death rate of activated AECs	1.65×10^{-2} day^{-1} [32]
d_H	death rate of HSCs	1.66×10^{-2} day^{-1} estimated
d_{E_0}	death rate of inactivated AECs	1.65×10^{-2} day^{-1} [32]
$d_{E_0 T}$	death rate of AECs	1.65×10^{-3} day^{-1} [32]
δ	increased death rate of AECs by injury	1×10^{-3} day^{-1} [31]
d_ρ	degradation rate of ECM	0.37 day^{-1} [32]
d_{H_A}	degradation rate of HA	0.1 day^{-1} estimated
d_P	degradation rate of MCP-1	1.73 day^{-1}[32]
d_{PM}	internalization rate of MCP-1 by M1 macrophages	2.08×10^{-4} day^{-1}[32]
d_G	degradation rate of PDGF	3.84 day^{-1} [32]
d_{QQ_r}	binding rate of MMP to TIMP	4.98×10^5 $cm^3 g^{-1}$ day^{-1} [32]
$d_{Q_r Q}$	binding rate of TIMP to MMP	1.04×10^6 $cm^3 g^{-1}$ day^{-1} [32]
d_Q	degradation rate of MMP	4.32 day^{-1}[32]
d_{Q_r}	degradation rate of TIMP	21.6 day^{-1} [32]
$d_{\rho Q}$	degradation rate of ECM due to MMP	2.59×10^5 $cm^3 g^{-1}$ day^{-1} [32]
d_{T_β}	degradation rate of TGF-β	3.33×10^2 day^{-1} [32]
d_f	death rate of fibroblasts	1.66×10^{-2} day^{-1} [32]
d_m	death rate of myofibroblasts	1.66×10^{-2} day^{-1} [32]
d_{T_α}	degradation rate of TNF-α	55.45 day^{-1} [33]
d_{I_2}	degradation rate of IL-2	2.376 day^{-1} [33]
d_{I_4}	degradation rate of IL-4	50 day^{-1} [33]
$d_{I_{10}}$	degradation rate of IL-10	8.32 day^{-1} [33]
$d_{I_{12}}$	degradation rate of IL-12	1.38 day^{-1} [33]
$d_{I_{13}}$	degradation rate of IL-13	12.47 day^{-1} [33]
d_{I_γ}	degradation rate of IFN-γ	2.16 day^{-1} [33]

[12] D. L. Clarke, A. M. Carruthers, T. Mustelin and L. A. Murray, Matrix regulation of idiopathic pulmonary fibrosis: The role of enzymes, *Fibrogenesis Tissue Repair*, **6** (2013), 20.

[13] M. K. Connolly, A. S. Bedrosian, J. Mallen-St Clair, A. P. Mitchell, J. Ibrahim, A. Stroud, H. L. Pachter, D. Bar-Sagi, A. B. Frey and G. Miller, In liver fibrosis, dendritic cells govern hepatic inflammation in mice via TNF-alpha, *J. Clin. Invest.*, **119** (2009), 3213–3225.

[14] Z. D. Daniil, E. Papageorgiou, A. Koutsokera, K. Kostikas, T. Kiropoulos and et al, Serum levels of oxidative stress as a marker of disease severity in idiopathic pulmonary fibrosis, *Pulm Pharmacol Ther*, **21** (2008), 26–31.

[15] J. Day, A. Friedman and L. S. Schlesinger, Modeling the immune rheostat of macrophages in the lung in response to infection, *Proc. Natl. Acad. Sci. U.S.A.*, **106** (2009), 11246–11251.

[16] P. Deepak, S. Kumar, D. Kishore and A. Acharya, IL-13 from Th2-type cells suppresses induction of antigen-specific Th1 immunity in a T-cell lymphoma, *Int. Immunol.*, **22** (2010), 53–63.

[17] J. A. Dranoff and R. G. Wells, Portal fibroblasts: Underappreciated mediators of biliary fibrosis, *Hepatology*, **51** (2010), 1438–1444.

Table 4. Parameters' description and value

Parameter	Description	Value
χ_P	chemotactic sensitivity parameter by MCP-1	$10\ cm^5 g^{-1}\ \text{day}^{-1}$ [32]
A_H	HSC proliferation	$3.32 \times 10^{-5}\ g/cm^3\ \text{day}^{-1}$ estimated
A_{E0}	intrinsic AEC proliferation	$1.65 \times 10^{-3}\ g/cm^3\ \text{day}^{-1}$ estimated
K_G	PDGF saturation for activation of myofibroblasts	$1.5 \times 10^{-8}\ gcm^{-3}$ [32]
K_{T_β}	TGF-β saturation for apoptosis of AECs	$1 \times 10^{-10}\ gcm^{-3}$ [32]
K_P	MCP-1 saturation for influx of macrophages	$5 \times 10^{-9}\ gcm^{-3}$ [32]
K_{T_α}	TNF-α saturation	$5 \times 10^{-7}\ gcm^{-3}$ [29]
$K_{I_{13}}$	IL-13 saturation	$2 \times 10^{-7}\ g/cm^3$ [29]
K_{H_A}	HA saturation	$2 \times 10^{-3}\ g/ml$ estimated
K_{T_1}	Th1 cell saturation	$1 \times 10^{-1}\ g/ml$ [33]
K_{I_γ}	IFN-γ saturation	$2 \times 10^{-7}\ gcm^{-3}$ [33]
K_{I_2}	IL-2 saturation	$5 \times 10^{-7}\ g/cm^3$ [33]
K_{I_4}	IL-4 saturation	$2 \times 10^{-7}\ g/cm^3$ [33]
$K_{I_{10}}$	IL-10 saturation	$2 \times 10^{-7}\ g/cm^3$ [29]
$K_{I_{12}}$	IL-12 saturation	$1.5 \times 10^{-5}\ g/cm^3$ [29]
$K_{I_{13}}$	IL-13 saturation	$2 \times 10^{-7}\ g/cm^3$ [29]
K_E	AEC saturation	$0.1\ g/cm^3$ [31]
ρ_0	ECM saturation	$10^{-2}\ gcm^{-3}$ [32]
ρ^*	ECM density in health	$3.26 \times 10^{-3}\ gcm^{-3}$ [31]
E^*	TEC density in health	$0.799\ gcm^{-3}$ [31]
f^*	fibroblast density in health	$4.75 \times 10^{-3}\ gcm^{-3}$ [31]
M_0	source/influx of macrophages from blood	$5 \times 10^{-5}\ gcm^{-3}$ [32]
β	influx rate of macrophages into interstitium	$0.2\ cm^{-1}$ [32]
A_{M_2}	Source term of M2	0.05 [29]
K_{M_1}	M1 saturation	0.5 [15]
K_{M_2}	M2 saturation	1 [15]
K_p	MCP-1 saturation	5×10^{-9} [32]
E_0	TEC saturation	$0.1\ g/ml$ estimated
ρ_0	ECM saturation	$10^{-2}\ g/ml$ [29]
T_0	T cells saturation	$3 \times 10^{-5}\ g/ml$ [30, 30]

[18] J. S. Duffield, Macrophages and immunologic inflammation of the kidney, *Semin. Nephrol.*, **30** (2010), 234–254.

[19] H. L. Fallatah, Noninvasive biomarkers of liver fibrosis: An overview, *Adva. in Hepa.*, **2014** (2014), Article ID 357287, 15pp.

[20] J. M. Fan, Y. Y. Ng, P. A. Hill, D. J. Nikolic-Paterson, W. Mu, R. C. Atkins and H. Y. Lan, Transforming growth factor-beta regulates tubular epithelial-myofibroblast transdifferentiation in vitro, *Kidney Int.*, **56** (1999), 1455–1467.

[21] S. Fichtner-Feigl, W. Strober, K. Kawakami, R. K. Puri and A. Kitani, IL-13 signaling through the IL-13alpha2 receptor is involved in induction of TGF-beta1 production and fibrosis, *Nat. Med.*, **12** (2006), 99–106.

[22] S. L. Friedman, Hepatic stellate cells: Protean, multifunctional, and enigmatic cells of the liver, *Physiol. Rev.*, **88** (2008), 125–172.

[23] R. M. Greco, J. A. Iocono and H. P. Ehrlich, Hyaluronic acid stimulates human fibroblast proliferation within a collagen matrix, *J. Cell. Physiol.*, **177** (1998), 465–473.

[24] J. Guechot, L. Serfaty, A. M. Bonnand, O. Chazouilleres, R. E. Poupon and R. Poupon, Prognostic value of serum hyaluronan in patients with compensated HCV cirrhosis, *J. Hepatol.*, **32** (2000), 447–452.

[25] M. F. Hadi, E. A. Sander, J. W. Ruberti and V. H. Barocas, Simulated remodeling of loaded collagen networks via strain-dependent enzymatic degradation and constant-rate fiber growth, *Mech Mater*, **44** (2012), 72–82.

[26] P. Halfon, M. Bourliere, G. Penaranda, R. Deydier, C. Renou, D. Botta-Fridlund, A. Tran, I. Portal, I. Allemand, A. Rosenthal-Allieri and D. Ouzan, Accuracy of hyaluronic acid level for predicting liver fibrosis stages in patients with hepatitis C virus, *Comp Hepatol*, **4** (2005), 6.

[27] L. Hammerich and F. Tacke, Role of gamma-delta T cells in liver inflammation and fibrosis, *World J Gastrointest Pathophysiol*, **5** (2014), 107–113.

[28] A. Hancock, L. Armstrong, R. Gama and A. Millar, Production of interleukin 13 by alveolar macrophages from normal and fibrotic lung, *Am. J. Respir. Cell Mol. Biol.*, **18** (1998), 60–65.

[29] W. Hao, E. D. Crouser and A. Friedman, Mathematical model of sarcoidosis, *Proc. Natl. Acad. Sci. U.S.A.*, **111** (2014), 16065–16070.

[30] W. Hao and A. Friedman, The LDL-HDL profile determines the risk of atherosclerosis: A mathematical model, *PLoS ONE*, **9** (2014), e90497.

[31] W. Hao, A. Friedman and C. Marsh, A mathematical model of idiopathic pulmonary fibrosis, *Plos One*, 10 (2015), e0135097.

[32] W. Hao, B. H. Rovin and A. Friedman, Mathematical model of renal interstitial fibrosis, *Proc. Natl. Acad. Sci. U.S.A.*, **111** (2014), 14193–14198.

[33] W. Hao, L. S. Schlesinger and A. Friedman, Modeling granulomas in response to infection in the lung, *PLoS ONE*, **11** (2016), e0148738.

[34] E. L. Herzog and R. Bucala, Fibrocytes in health and disease, *Exp. Hematol.*, **38** (2010), 548–556.

[35] K. Iyonaga, M. Takeya, N. Saita, O. Sakamoto, T. Yoshimura, M. Ando and K. Takahashi, Monocyte chemoattractant protein-1 in idiopathic pulmonary fibrosis and other interstitial lung diseases, *Hum. Pathol.*, **25** (1994), 455–463.

[36] C. Jakubzick, E. S. Choi, B. H. Joshi, M. P. Keane, S. L. Kunkel and et al, Therapeutic attenuation of pulmonary fibrosis via targeting of IL-4- and IL-13-responsive cells, *J. Immunol.*, **171** (2003), 2684–2693.

[37] C. A. Janeway, T. P., W. M. and M. J. Shlomchik, *Immunobiology, 5th edition, The Immune System in Health and Disease*, 2001.

[38] R. Khan and R. Sheppard, Fibrosis in heart disease: Understanding the role of transforming growth factor-beta in cardiomyopathy, valvular disease and arrhythmia, *Immunology*, **118** (2006), 10–24.

[39] N. Kikuchi, Y. Ishii, Y. Morishima, Y. Yageta, N. Haraguchi, K. Itoh, M. Yamamoto and N. Hizawa, Nrf2 protects against pulmonary fibrosis by regulating the lung oxidant level and Th1/Th2 balance, *Respir. Res.*, **11** (2010), 31.

[40] C. R. Kliment and T. D. Oury, Oxidative stress, extracellular matrix targets, and idiopathic pulmonary fibrosis, *Free Radic. Biol. Med.*, **49** (2010), 707–717.

[41] P. Kong, P. Christia and N. G. Frangogiannis, The pathogenesis of cardiac fibrosis, *Cell. Mol. Life Sci.*, **71** (2014), 549–574.

[42] T. Lan, T. Kisseleva and D. A. Brenner, Deficiency of NOX1 or NOX4 prevents liver inflammation and fibrosis in mice through inhibition of hepatic stellate cell activation, *PLoS ONE*, **10** (2015), e0129743.

[43] A. Leask, TGFbeta, cardiac fibroblasts, and the fibrotic response, *Cardiovasc. Res.*, **74** (2007), 207–212.

[44] A. Leask and D. J. Abraham, TGF-beta signaling and the fibrotic response, *FASEB J.*, **18** (2004), 816–827.

[45] B. Lee, X. Zhou, K. Riching, K. W. Eliceiri, P. J. Keely, S. A. Guelcher, A. M. Weaver and Y. Jiang, A three-dimensional computational model of collagen network mechanics, *PLoS ONE*, **9** (2014), e111896.

[46] C. Liedtke, T. Luedde, T. Sauerbruch, D. Scholten, K. Streetz, F. Tacke, R. Tolba, C. Trautwein, J. Trebicka and R. Weiskirchen, Experimental liver fibrosis research: Update on animal models, legal issues and translational aspects, *Fibrogenesis Tissue Repair*, **6** (2013), 19.

[47] P. Lijnen and V. Petrov, Transforming growth factor-beta 1-induced collagen production in cultures of cardiac fibroblasts is the result of the appearance of myofibroblasts, *Methods Find Exp Clin Pharmacol*, **24** (2002), 333–344.

[48] L. Liu, P. Kou, Q. Zeng, G. Pei, Y. Li, H. Liang, G. Xu and S. Chen, CD4+ T Lymphocytes, especially Th2 cells, contribute to the progress of renal fibrosis, *Am. J. Nephrol.*, **36** (2012), 386–396.

[49] T. Liu, X. Wang, M. A. Karsdal, D. J. Leeming and F. Genovese, Molecular serum markers of liver fibrosis, *Biomark Insights*, **7** (2012), 105–117.

[50] Y. Liu, X. M. Wen, E. L. Lui, S. L. Friedman, W. Cui, N. P. Ho, L. Li, T. Ye, S. T. Fan and H. Zhang, Therapeutic targeting of the PDGF and TGF-beta-signaling pathways in hepatic stellate cells by PTK787/ZK22258, *Lab. Invest.*, **89** (2009), 1152–1160.

[51] S. Lo Re, D. Lison and F. Huaux, CD4+ T lymphocytes in lung fibrosis: Diverse subsets, diverse functions, *J. Leukoc. Biol.*, **93** (2013), 499–510.

[52] N. J. Lomas, K. L. Watts, K. M. Akram, N. R. Forsyth and M. A. Spiteri, Idiopathic pulmonary fibrosis: immunohistochemical analysis provides fresh insights into lung tissue remodelling with implications for novel prognostic markers, *Int J Clin Exp Pathol*, **5** (2012), 58–71.

[53] P. Lu, K. Takai, V. M. Weaver and Z. Werb, Extracellular matrix degradation and remodeling in development and disease, *Cold Spring Harb Perspect Biol*, **3** (2011), 1–25.

[54] I. G. Luzina, N. W. Todd, A. T. Iacono and S. P. Atamas, Roles of T lymphocytes in pulmonary fibrosis, *J. Leukoc. Biol.*, **83** (2008), 237–244.

[55] K. J. Maloy and F. Powrie, Intestinal homeostasis and its breakdown in inflammatory bowel disease, *Nature*, **474** (2011), 298–306.

[56] S. Marino, I. B. Hogue, C. J. Ray and D. E. Kirschner, A methodology for performing global uncertainty and sensitivity analysis in systems biology, *J. Theor. Biol.*, **254** (2008), 178–196.

[57] D. I. McRitchie, N. Isowa, J. D. Edelson, A. M. Xavier, L. Cai and et al, Production of tumour necrosis factor alpha by primary cultured rat alveolar epithelial cells, *Cytokine*, **12** (2000), 644–654.

[58] D. L. Motola, P. Caravan, R. T. Chung and B. C. Fuchs, Noninvasive biomarkers of liver fibrosis: Clinical applications and future directions, *Curr Pathobiol Rep*, **2** (2014), 245–256.

[59] L. A. Murray, Q. Chen, M. S. Kramer, D. P. Hesson, R. L. Argentieri and et. al., TGF-beta driven lung fibrosis is macrophage dependent and blocked by Serum amyloid P, *Int. J. Biochem. Cell Biol.*, **43** (2011), 154–162.

[60] S. Nakatsuji, J. Yamate and S. Sakuma, Macrophages, myofibroblasts, and extracellular matrix accumulation in interstitial fibrosis of chronic progressive nephropathy in aged rats, *Vet. Pathol.*, **35** (1998), 352–360.

[61] Y. E. Nassef, M. M. Shady, E. M. Galal and M. A. Hamed, Performance of diagnostic biomarkers in predicting liver fibrosis among hepatitis C virus-infected Egyptian children, *Mem. Inst. Oswaldo Cruz*, **108** (2013), 887–893.

[62] Q. H. Nie, Y. F. Zhang, Y. M. Xie, X. D. Luo, B. Shao, J. Li and Y. X. Zhou, Correlation between TIMP-1 expression and liver fibrosis in two rat liver fibrosis models, *World J. Gastroenterol.*, **12** (2006), 3044–3049.

[63] D. J. Nikolic-Paterson, CD4+ T cells: A potential player in renal fibrosis, *Kidney Int.*, **78** (2010), 333–335.

[64] A. Pellicoro, P. Ramachandran, J. P. Iredale and J. A. Fallowfield, Liver fibrosis and repair: Immune regulation of wound healing in a solid organ, *Nat. Rev. Immunol.*, **14** (2014), 181–194.

[65] M. Perepelyuk, M. Terajima, A. Y. Wang, P. C. Georges, P. A. Janmey, M. Yamauchi and R. G. Wells, Hepatic stellate cells and portal fibroblasts are the major cellular sources of collagens and lysyl oxidases in normal liver and early after injury, *Am. J. Physiol. Gastrointest. Liver Physiol.*, **304** (2013), G605–g614.

[66] M. P. Rastaldi, F. Ferrario, L. Giardino, G. Dell'Antonio, C. Grillo, P. Grillo, F. Strutz, G. A. Muller, G. Colasanti and G. D'Amico, Epithelial-mesenchymal transition of tubular epithelial cells in human renal biopsies, *Kidney Int.*, **62** (2002), 137–146.

[67] E. F. Redente, R. C. Keith, W. Janssen, P. M. Henson, L. A. Ortiz, G. P. Downey, D. L. Bratton and D. W. Riches, Tumor necrosis factor-alpha accelerates the resolution of established pulmonary fibrosis in mice by targeting profibrotic lung macrophages, *Am. J. Respir. Cell Mol. Biol.*, **50** (2014), 825–837.

[68] S. D. Ricardo, H. van Goor and A. A. Eddy, Macrophage diversity in renal injury and repair, *J. Clin. Invest.*, **118** (2008), 3522–3530.

[69] J. Rosenbloom, S. V. Castro and S. A. Jimenez, Narrative review: Fibrotic diseases: Cellular and molecular mechanisms and novel therapies, *Ann. Intern. Med.*, **152** (2010), 159–166.

[70] N. Sakai and A. M. Tager, Fibrosis of two: Epithelial cell-fibroblast interactions in pulmonary fibrosis, *Biochim. Biophys. Acta*, **1832** (2013), 911–921.

[71] M. Selman and A. Pardo, Role of epithelial cells in idiopathic pulmonary fibrosis: From innocent targets to serial killers, *Proc. Am. Thorac. Soc.*, **3** (2006), 364–372.

[72] M. Selman and A. Pardo, Revealing the pathogenic and aging-related mechanisms of the enigmatic idiopathic pulmonary fibrosis. an integral model, *Am. J. Respir. Crit. Care Med.*, **189** (2014), 1161–1172.

[73] G. Shiha, Serum hyaluronic acid: A promising marker of hepatic fibrosis in chronic hepatitis B, *Saudi J Gastroenterol*, **14** (2008), 161–162.

[74] Y. Shimizu, H. Kuwabara, A. Ono, S. Higuchi, T. Hisada, K. Dobashi, M. Utsugi, Y. Mita and M. Mori, Intracellular Th1/Th2 balance of pulmonary CD4(+) T cells in patients with active interstitial pneumonia evaluated by serum KL-6, *Immunopharmacol Immunotoxicol*, **28** (2006), 295–304.

[75] M. S. Simonson and F. Ismail-Beigi, Endothelin-1 increases collagen accumulation in renal mesangial cells by stimulating a chemokine and cytokine autocrine signaling loop, *J. Biol. Chem.*, **286** (2011), 11003–11008.

[76] F. Strutz and M. Zeisberg, Renal fibroblasts and myofibroblasts in chronic kidney disease, *J. Am. Soc. Nephrol.*, **17** (2006), 2992–2998.

[77] F. Strutz, M. Zeisberg, A. Renziehausen, B. Raschke, V. Becker, C. van Kooten and G. Muller, TGF-beta 1 induces proliferation in human renal fibroblasts via induction of basic fibroblast growth factor (FGF-2), *Kidney Int.*, **59** (2001), 579–592.

[78] F. Tacke and H. W. Zimmermann, Macrophage heterogeneity in liver injury and fibrosis, *J. Hepatol.*, **60** (2014), 1090–1096.

[79] N. Takemoto, N. Koyano-Nakagawa, T. Yokota, N. Arai, S. Miyatake and K. Arai, Th2-specific DNase I-hypersensitive sites in the murine IL-13 and IL-4 intergenic region, *Int. Immunol.*, **10** (1998), 1981–1985.

[80] R. J. Tan and Y. Liu, Macrophage-derived TGF-beta in renal fibrosis: not a macro-impact after all, *Am. J. Physiol. Renal Physiol.*, **305** (2013), F821–822.

[81] T. T. Tapmeier, A. Fearn, K. Brown, P. Chowdhury, S. H. Sacks, N. S. Sheerin and W. Wong, Pivotal role of CD4+ T cells in renal fibrosis following ureteric obstruction, *Kidney Int.*, **78** (2010), 351–362.

[82] A. L. Tatler and G. Jenkins, TGF-beta activation and lung fibrosis, *Proc. Am. Thorac. Soc.*, **9** (2012), 130–136.

[83] S. S. Veidal, M. A. Karsdal, E. Vassiliadis, A. Nawrocki, M. R. Larsen, Q. H. Nguyen, P. Hagglund, Y. Luo, Q. Zheng, B. Vainer and D. J. Leeming, MMP mediated degradation of type VI collagen is highly associated with liver fibrosis–identification and validation of a novel biochemical marker assay, *PLoS ONE*, **6** (2011), e24753.

[84] R. Venkayya, M. Lam, M. Willkom, G. Grunig, D. B. Corry and et al, The Th2 lymphocyte products IL-4 and IL-13 rapidly induce airway hyperresponsiveness through direct effects on resident airway cells, *Am. J. Respir. Cell Mol. Biol.*, **26** (2002), 202–208.

[85] T. Veremeyko, S. Siddiqui, I. Sotnikov, A. Yung and E. D. Ponomarev, IL-4/IL-13-dependent and independent expression of miR-124 and its contribution to M2 phenotype of monocytic cells in normal conditions and during allergic inflammation, *PLoS ONE*, **8** (2013), e81774.

[86] M. A. Vernon, K. J. Mylonas and J. Hughes, Macrophages and renal fibrosis, *Semin. Nephrol.*, **30** (2010), 302–317.

[87] T. Wada, K. Furuichi, N. Sakai, Y. Iwata, K. Kitagawa, Y. Ishida, T. Kondo, H. Hashimoto, Y. Ishiwata, N. Mukaida, N. Tomosugi, K. Matsushima, K. Egashira and H. Yokoyama, Gene therapy via blockade of monocyte chemoattractant protein-1 for renal fibrosis, *J. Am. Soc. Nephrol.*, **15** (2004), 940–948.

[88] T. Wada, H. Yokoyama, K. Matsushima and K. Kobayashi, Monocyte chemoattractant protein-1: does it play a role in diabetic nephropathy?, *Nephrol. Dial. Transplant.*, **18** (2003), 457–459.

[89] L. Wei, Immunological aspect of cardiac remodeling: T lymphocyte subsets in inflammation-mediated cardiac fibrosis, *Exp. Mol. Pathol.*, **90** (2011), 74–78.

[90] X. Weng, L. Wang, J. Wang, Y. Hu, H. Du, C. Xu, Y. Xing, X. Li, J. Xiao and Q. Zhang, Grain number, plant height, and heading date7 is a central regulator of growth, development, and stress response, *Plant Physiol.*, **164** (2014), 735–747.

[91] T. A. Wynn, Fibrotic disease and the T(H)1/T(H)2 paradigm, *Nat. Rev. Immunol.*, **4** (2004), 583–594.

[92] L. Xiao, Y. Du, Y. Shen, Y. He, H. Zhao and Z. Li, TGF-beta 1 induced fibroblast proliferation is mediated by the FGF-2/ERK pathway, *Front Biosci (Landmark Ed)*, **17** (2012), 2667–2674.

[93] A. Yates, R. Callard and J. Stark, Combining cytokine signalling with T-bet and GATA-3 regulation in Th1 and Th2 differentiation: a model for cellular decision-making, *J. Theor. Biol.*, **231** (2004), 181–196.

[94] H. Zhao, Y. Dong, X. Tian, T. K. Tan, Z. Liu, Y. Zhao, Y. Zhang, D. C. h. Harris and G. Zheng, Matrix metalloproteinases contribute to kidney fibrosis in chronic kidney diseases, *World J Nephrol*, **2** (2013), 84–89.

[95] J. Zhao, N. Tang, K. Wu, W. Dai, C. Ye, J. Shi, J. Zhang, B. Ning, X. Zeng and Y. Lin, MiR-21 simultaneously regulates ERK1 signaling in HSC activation and hepatocyte EMT in hepatic fibrosis, *PLoS ONE*, **9** (2014), e108005.

E-mail address: `afriedman@math.osu.edu`
E-mail address: `wxh64@psu.edu`